Simulation of the observation of galaxy clusters via the thermal Sunyaev-Zel'dovich effect with the NIKA camera
(Research Note)

R. Adam[1], J. F. Macías-Pérez[1], F. X. Désert[2], N. Ponthieu[2], B. Comis[1], A. Benoit[3], M. Calvo[3], A. Catalano[1], and A. Monfardini[3]

[1] Laboratoire de Physique Subatomique et de Cosmologie, Université Joseph Fourier Grenoble 1, CNRS/IN2P3, Institut Polytechnique de Grenoble, 53, rue des Martyrs, Grenoble, France
[2] IPAG, Observatoire de Grenoble, BP 53, 38041 Grenoble, France
[3] Institut Néel, CNRS & Université Joseph Fourier, BP 166, 38042 Grenoble, France

October 2012

ABSTRACT

Context. The thermal Sunyaev-Zel'dovich (tSZ) effect describes the Compton inverse scatter of Cosmic Microwave Background (CMB) photons on hot electrons in galaxy clusters. It can be used to measure the mass of clusters and therefore to constrain the cosmological parameters. It requires a high resolution instrument in order to extract the pressure profile of the observed cluster. The New IRAM KIDs Array (NIKA) appears to be an ideal instrument to do so since it has a resolution of about 12 arcsec.
Aims. The objective is to use the simulation pipeline of the NIKA camera in order to estimate the capability of the camera concerning the observation of galaxy clusters via the tSZ effect.
Methods. We report here the result of a simulation of the observation of galaxy clusters with the NIKA camera. This includes the reconstruction of the maps and the pressure profile observed.
Results. The simulation of the observation of galaxy clusters with the NIKA camera has shown that the performances of the prototype of NIKA are already good enough to image massive clusters and measure their pressure profile with a good accuracy, and within a reasonable time of observation.
Conclusions. The NIKA camera should be a powerful instrument for tSZ measurements at high resolution. KIDs arrays have been proved to be competitive detectors for millimeter waves astronomy. The final camera (2014) should have a sensitivity as good as (or even better than) the current experiments dedicated to observation of the tSZ effect, such as the South Pole Telescope, with a resolution four times better.

Key words. Kinetic Inductance Detectors – The New IRAM KIDs Array – thermal Sunyaev-Zel'dovich effect – Simulation

1. Introduction

The standard model of cosmology seems to be in good agreement with observations. However, in this model only 4% of the energy content of the Universe is known (Larson et al. (2011)); the so-called dark matter and dark energy account for the missing part. Probing galaxy clusters can give strong constraints on dark matter and dark energy (Benson et al. (2011)). Indeed, these clusters are the largest gravitationally bound objects in the Universe, decoupled from its expansion, and their formation strongly depends on the content and the history of the Universe (Buchert (2008)). The distribution of clusters per unit mass and redshift can be of particular interest.

Galaxy clusters are classically probed using methods such as gravitational lensing of background galaxies (Tyson et al. (1990)), measurement of X radiation emitted via bremsstrahlung from hot electrons in the Intra Cluster Medium (ICM) (Borgani et al. (2011)), or directly using the galaxies within the cluster (optical, radio and infrared observations). The Sunyaev-Zel'dovich (tSZ) effect can be used as a complementary and powerful method for probing galaxy clusters (Carlstrom et al. (2002)). It describes the inverse Compton Scattering of Cosmic Microwave Background (CMB) photons on hot electrons in the ICM of galaxy clusters (Sunyaev & Zel'dovich (1972), Sunyaev & Zel'dovich (1980)). The blackbody spectrum of CMB photons is shifted to higher frequencies, leading to secondary temperature anisotropies in the CMB (Birkinshaw (1999)). The main interest of tSZ observation relies on the fact that it does not depend on the redshift, apart from the angular size of clusters, since the observable is not the cluster itself but its imprint in the CMB. The measurement of the mass of the clusters requires an accurate reconstruction of the pressure profile and therefore a high resolution instrument.

The resolutions of current instruments observing the tSZ effect are rather poor: larger than 5 arcmin for the Planck satellite and about 1 arcmin for the South Pole Telescope (SPT) (Carlstrom et al. (2011)), the Atacama Cosmology Telescope (ACT) (Kosowsky (2003)), and the Arcminute Microkelvin Imager (AMI) (AMI Consortium et al. (2012)). The New IRAM KIDs Array (NIKA) is a new camera based on Kinetic Inductance Detectors (KIDs) (Calvo et al. (2010)) with a resolution of about 12 arcsec, in development for millimeter waves astronomy (Monfardini et al. (2011)). It appears to be an ideal instrument for tSZ observation. NIKA could be used as a follow up of Planck which has detected hundreds of clusters during a full sky survey (Planck Collaboration et al. (2011), Planck et al. (2012)). NIKA has already been successfully tested during four campaigns (see Monfardini et al. (2010) and Monfardini et al. (2011)) at the Institut de RadioAstronomie Millimétrique (IRAM) 30-meters telescope at Pico Veleta, Spain. The final camera should be operational in 2014.

This note presents the use of the simulation of the NIKA camera for the observation of the tSZ effect. It is divided into five parts. In the first one, we describe the physics of the tSZ effect. Then, we briefly present the simulation of the Time Ordered Information (TOI) obtained with NIKA for a run of observation at the IRAM 30-meters telescope at Pico Veleta (the full description can be found in Adam et al. (2012)). In the next part, we expose the way the mapmaking and the profile reconstruction has been performed. Finally, the results are presented and discussed.

2. The Sunyaev Zel'dovich effect

When traveling in the Universe, CMB photons might encounter galaxy cluster. These clusters contain free electrons on which CMB photons can inverse Compton scatter (Sunyaev & Zel'dovich (1972), Sunyaev & Zel'dovich (1980)). The motion of electrons in galaxy clusters can be approximated by two contributions. The former is due to the thermal motion of hot electrons, leading to the thermal Sunyaev-Zel'dovich effect (tSZ). The later arises when the relative motion of the cluster with respect to the CMB reference frame is non zero, this accounts for the kinetic Sunyaev-Zel'dovich (kSZ) effect. We will focus here on the tSZ effect and ignore the kSZ effect which has not been taken into account in the simulation that we present, because of its much smaller contribution.

In the non relativistic limit[1] of the tSZ effect, the distortion of the CMB black body spectrum is given by (Birkinshaw (1999))

$$f(x) = x \coth\left(\frac{x}{2}\right) - 4 \tag{1}$$

where $x = \frac{h\nu}{k_{\mathrm{B}} T_{\mathrm{CMB}}}$ is the dimensionless frequency; h is the Planck constant, k_{B} the Boltzmann constant, ν the observation frequency and T_{CMB} the temperature of the CMB. The temperature anisotropies can be written as

$$\frac{\delta T_{\mathrm{CMB}}}{T_{\mathrm{CMB}}} = y f(x) \tag{2}$$

where y is the Compton parameter which gives a measure of the integrated electronic pressure P_{e} along the line-of-sigh.

$$y = \frac{\sigma_{\mathrm{T}}}{m_{\mathrm{e}} c^2} \int P_{\mathrm{e}} dl \tag{3}$$

with σ_{T} the Thomson cross section, m_{e} the electron mass and c the speed of light.

In this simulation, we chose to model the pressure profile of observed clusters by the generalized Navaro Frenk and White (gNFW) pressure profile (Nagai et al. (2007)), which is expected to describe the cluster pressure out to a significant fraction of the virial radius. This profile is given by

$$P(r) = P_{500} \frac{P_0}{\left(\frac{r}{r_{\mathrm{s}}}\right)^{\gamma} \left(1 + \left(\frac{r}{r_{\mathrm{s}}}\right)^{\alpha}\right)^{\frac{\beta-\gamma}{\alpha}}} \tag{4}$$

where P_0 is a normalizing constant; α, β and γ set the slope at intermediate, large and small radii respectively; r_{s} is the characteristic radius, it can be written as $r_{\mathrm{s}} = r_{500}/c_{500}$ with r_{500} the radius within which the mean density of the cluster is equal to 500 times the critical density of the Universe at the corresponding redshift and c_{500} a parameter which characterize the gas concentration. The parameter P_{500} is the average pressure within the radius r_{500}, it is related to the average mass within the same radius, M_{500}, by the relation (Arnaud et al. (2010))

$$P_{500} = 1.65 \times 10^{-3} h(z)^{8/3} \left(\frac{M_{500}}{3 \times 10^{14} M_{\odot}}\right)^{2/3} h_{70}^{2/3} \ \mathrm{KeV.cm^{-3}} \tag{5}$$

where $h(z)$ is the ratio of the Hubble constant at the redshift z and the Hubble constant today, $M_{\odot}$ the mass of the sun and h_{70} the Hubble constant today normalized by 70 km/s/Mpc. We finally define $\theta_{\mathrm{s}} = r_{\mathrm{s}}/D_{\mathrm{A}}$ where D_{A} is the angular distance of the cluster. The stacked fit of *Planck data* gives $(P_0, \alpha, \beta, \gamma, c_{500}) = (6.41, 1.33, 4.13, 0.31, 1.81)$ (Planck Collaboration et al. (2012)).

Observations of galaxy clusters via the tSZ effect are characterized by a diminution of the temperature of the CMB for frequencies lower than $\simeq 217$ GHz (*i.e.* $f(x) < 0$) and a rise for higher frequencies (*i.e.* $f(x) > 0$), the tSZ effect has no impact on the CMB at $\simeq 217$ GHz (*i.e.* $f(x) = 0$). Observing these temperature anisotropies in the CMB can be used to compute the integrated y parameter out to a given radius, this quantity is proportional to the total thermal energy of the cluster and is therefore expected to give a low scatter estimate of the total mass. In addition, tSZ observations are complementary to X-ray observations because the tSZ flux is proportional to the electron number density while the X-ray flux is proportional to the electron number density squared, so X-ray measurements are rather sensitive to the core of clusters and tSZ to clusters out to larger radii. Finally, the tSZ effect does only depend on the redshift via the angular size of clusters, so the reconstruction of the masses of large redshift clusters requires a high resolution instrument. Observations of clusters via the tSZ effect should give important constraints on cosmology via the measurement of the mass distribution in the Universe (Benson et al. (2011)).

3. Simulation of the observation of galaxy clusters via the tSZ effect with NIKA

3.1. Simulation of the tSZ flux

We simulate the pressure profile of galaxy clusters using the gNFW pressure profile given by Equation 4. By integrating along the line-of-sight we obtain the Compton parameter y from which we build the Rayleigh-Jeans temperature map. We then convolute the map with a 15 arcsec FWHM Gaussian to account for the instrumental lobe, such that all detectors are assumed to have the same resolution. All other possible astrophysical sources are neglected.

3.2. Time Ordered Information

The description of the simulation of the camera, its operating principle and the sources of noise can be found in Adam et al. (2012). TOIs are obtained by sampling the observed region of the sky using a realistic serpentine like scan. This leads to temperature Rayleigh-Jeans TOIs to which we add the atmospheric noise. The measured quantity used to probed the optical power is the shift of the resonance frequency of the detectors, as described in Adam et al. (2012), it is given by

$$\begin{aligned} \delta {f_0^{\mathrm{meas}}}_k(t) = \Gamma_\nu \lambda_k \left[P_k(x_k, y_k, t) S_{\mathrm{SZ}}(x_k, y_k) + S_{\mathrm{atmo}}(x_k, y_k, t)\right] \\ + \mu_k N_{cor}(t) + \chi_k N_{dec}(t) \end{aligned} \tag{6}$$

where k labels the KID, $P_k(x_k, y_k, t)$ is the pointing matrix, $S_{\mathrm{SZ}}(x_k, y_k)$ the tSZ signal, $S_{\mathrm{atmo}}(x_k, y_k, t)$ the atmospheric noise, $N_{cor}(t)$ the correlated noise and $N_{dec}(t)$ the non correlated noise.

[1] In the simulation presented here, relativistic corrections (Itoh et al. (2001)) have been neglected, therefore they will be ignored here.

The coefficients λ_k are known experimentally and give the calibration, and the coefficients μ_k and χ_k account for the different amplitudes of the instrumental noises. The coefficient Γ_ν give the mean shift of the resonance frequency to K_{RJ} calibration: $\Gamma_{140\ GHz} = 670$ Hz.K_{RJ}^{-1} and $\Gamma_{220\ GHz} = 500$ Hz.K_{RJ}^{-1}.

4. Data reduction and map-making

In practice the tSZ signal is completely drown within the different sources of noise, in particular the atmospheric noise. In order to recover the tSZ signal, we use the following method. For simplicity in the notations, let the $\delta f_0^{\mathrm{meas}}{}_k(t)$ TOIs for the detector number k and the observing frequency ν, after calibration, be $d_k(\nu; t)$.

4.1. $I - Q$ decorrelation

The correlated part of the noise that we want to subtract is

$$d_{\mathrm{cor},k}(\nu, t) = P_k(x_k, y_k, t)\, S_{\mathrm{atmo}}(x_k, y_k, t) + \mu'_k N_{\mathrm{cor}}(t) \tag{7}$$

with $\mu'_k = \mu_k/\lambda_k$.

In practice, the method used to measure the shift of the resonance frequency $\delta f_0^{\mathrm{meas}}{}_k(t)$ does not make sense in the case of OFF resonance tones (Adam et al. (2012)), such that the correlated electronic noise cannot be well estimated from $\delta f_0^{\mathrm{meas}}{}_k(t)$. In order to remove properly this noise from the TOIs, we estimate it directly in the $I_k(t)$, $Q_k(t)$, $\delta I_k(t)$ and $\delta Q_k(t)$ TOIs[2] using OFF resonance detectors, which are blind to optical signal.

The estimation of the correlated electronic noise within these quantities, $I_{\mathrm{cor}}(t)$, $Q_{\mathrm{cor}}(t)$, $\delta I_{\mathrm{cor}}(t)$, $\delta Q_{\mathrm{cor}}(t)$, is performed using the off resonance KIDs. It is given by

$$\begin{cases} \hat{I}_{\mathrm{cor}}(t) = \frac{1}{N_{\mathrm{off}}} \sum_{l=1}^{N_{\mathrm{off}}} \left[I_{\mathrm{off};l}(t) - < I_{\mathrm{off};l}(t) >\right] \\ \hat{Q}_{\mathrm{cor}}(t) = \frac{1}{N_{\mathrm{off}}} \sum_{l=1}^{N_{\mathrm{off}}} \left[Q_{\mathrm{off};l}(t) - < Q_{\mathrm{off};l}(t) >\right] \\ \hat{\delta I}_{\mathrm{cor}}(t) = \frac{1}{N_{\mathrm{off}}} \sum_{l=1}^{N_{\mathrm{off}}} \left[\delta I_{\mathrm{off};l}(t) - < \delta I_{\mathrm{off};l}(t) >\right] \\ \hat{\delta Q}_{\mathrm{cor}}(t) = \frac{1}{N_{\mathrm{off}}} \sum_{l=1}^{N_{\mathrm{off}}} \left[\delta I_{\mathrm{off};l}(t) - < \delta I_{\mathrm{off};l}(t) >\right] \end{cases} \tag{8}$$

The $I(t)$, $Q(t)$, $\delta I(t)$, $\delta Q(t)$ TOIs are then decorrelated of this correlated electronic noise using a linear regression. The shift of the resonance frequency TOIs are then computed as described in Adam et al. (2012).

4.2. Plane atmosphere approximation

The atmospheric noise is well described in first approximation by a plane with changing amplitude and tilt, such that the correlated noise can be modeled, after removing the electronic noise in the $I - Q$ plane, by the following expression

$$d_{\mathrm{atmo},k}(\nu; t) = A_0(\nu; t) + A_1(\nu; t)\frac{x_k - x_0}{L_{\mathrm{NIKA}}} + A_2(\nu; t)\frac{y_k - y_0}{L_{\mathrm{NIKA}}} \tag{9}$$

where $A_0(\nu; t)$ give the global amplitude of the atmosphere and $A_{1,2}(\nu; t)$ the tilt. The size of the camera in the focal plane is L_{NIKA} and $(x_k - x_0, y_k - y_0)$ give the relative position of the detector k with respect to the center of the array (x_0, y_0). From equation 9, the estimation of the atmospheric noise is given by

$$\hat{A}_0(\nu; t) = \frac{1}{N_{\mathrm{KID}}} \sum_{k=1}^{N_{\mathrm{KID}}} d_k(\nu; t) \tag{10}$$

$$\hat{A}_1(\nu; t) = L_{\mathrm{NIKA}} \frac{\sum_{k=1}^{N_{\mathrm{KID}}} d_k(\nu; t)\,(x_k - x_0)}{\sum_{k=1}^{N_{\mathrm{KID}}} (x_k - x_0)^2} \tag{11}$$

$$\hat{A}_2(\nu; t) = L_{\mathrm{NIKA}} \frac{\sum_{k=1}^{N_{\mathrm{KID}}} d_k(\nu; t)\,(y_k - y_0)}{\sum_{k=1}^{N_{\mathrm{KID}}} (y_k - y_0)^2} \tag{12}$$

with N_{KID} the number of ON detectors. Since the atmospheric noise is proportional for the two observing frequency, it is estimated from the TOIs of the array at $\nu = 220$ GHz because it contains almost no tSZ signal. The correlated atmospheric noise is then estimated for the array at 140 GHz (which contains tSZ signal) by

$$\hat{d}_{\mathrm{atmo},k}(140\ \mathrm{GHz}; t) = \sum_{n=0}^{2} C_{n,k}\, \hat{A}_n(220\ \mathrm{GHz}; t) \tag{13}$$

where the coefficients $C_{n,k}$ are found with a linear regression.

4.3. Mapmaking

The estimated signal is then given, at $\nu = 140$ GHz, by

$$P_k(x, y, t)\, \hat{S}_{\mathrm{SZ},k}(x_k, y_k) = d_k(140\ \mathrm{GHz}; t) - \hat{d}_{\mathrm{atmo},k}(140\ \mathrm{GHz}; t) \tag{14}$$

In order to remove possible offsets in the TOIs, we subtract the mean value of the TOIs. The bias introduced is small since the tSZ signal is small with respect to the noise. Nevertheless, it is corrected as explained in the next section. Finally, we obtain the shift of the resonance frequency anisotropy maps by projecting and averaging the signal from all KIDs on a pixelated map at 140 GHz. The Γ_ν coefficient allows us to go from shift of the resonance frequency maps to temperature maps in Kelvin Rayleigh-Jeans, to CMB temperature anisotropies and to Compton parameter y maps.

4.4. Profile computation

For each map, we build the profile of the cluster by computing the average value of the Compton parameter y map for a set of concentric annuli with inner and outer radii set to the boundaries of radial bins. The radial coordinate corresponding to the Compton parameter y value is given by the average radial distance of the pixel considered. The offset introduced by setting the mean value of the TOI to naught is corrected by adding an offset to the final map (and profile), equal to the mean value of the map within a radius corresponding to twice the FWHW of the measured profile.

5. Results

We choose to simulate the clusters selected for possible observation during NIKA run 5, they are given in table 1. The fit of the pressure profile has been done using Chandra's data (Comis et al. (2011)), in which the parameters α and β have been fixed to the values obtained with the fit of the stacked profile, respectively to

[2] Respectively the real and imaginary parts of the transfer function associated to the KIDs, and their differential with respect to the change of the injected tones. See Calvo et al. (2012) or Adam et al. (2012) for more details.

Name	$P_0 \times P_{500}$ (10^{-12} Pa)	α	β	γ	r_s (kpc)	θ_s (arcsec)	z
RX J1347.5-1145	526.9 ± 80.8	0.9	5.0	-0.003 ± 0.047	406 ± 23	70 ± 4	0.4516
A2163	28.8 ± 4.5	0.9	5.0	-0.128 ± 0.045	1580 ± 170	474 ± 51	0.2030
A520	14.7 ± 2.0	0.9	5.0	-0.327 ± 0.047	1327 ± 93	398 ± 28	0.2030
A665	1.48 ± 0.21	0.9	5.0	0.448 ± 0.030	3198 ± 257	1047 ± 84	0.1818
A1689	30.8 ± 3.9	0.9	5.0	0.191 ± 0.033	661 ± 34	215 ± 11	0.1832
MACS J2228+2036	12.2 ± 1.5	0.9	5.0	0.166 ± 0.040	1032 ± 49	188 ± 9	0.4120
MS 0451.6-0305	7.3 ± 0.8	0.9	5.0	0.091 ± 0.042	886 ± 57	139 ± 9	0.5377
A697	13.3 ± 2.2	0.9	5.0	0.117 ± 0.042	1268 ± 111	297 ± 26	0.2820
MACS J0717.5+3745	100.0 ± 7.6	0.9	5.0	-0.435 ± 0.034	700 ± 26	109 ± 4	0.5460
MS 0016.9+1609	25.1 ± 2.8	0.9	5.0	-0.044 ± 0.037	995 ± 51	155 ± 8	0.5456

Table 1. List of clusters modeled using pressure profile fit with Chandra's data (Comis et al. (2011)). Note that α and β have been fixed to the values obtained with the stacked profile of Chandra's data.

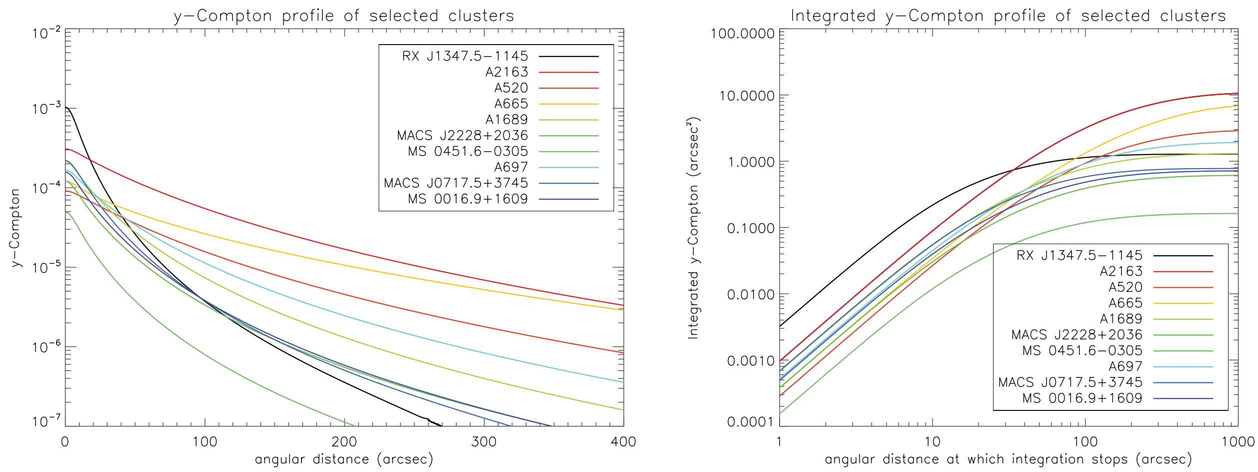

Fig. 1. Profiles of the simulated clusters according to the parameters given in table 1. The left panel gives the angular profile of the Compton parameter y simulated via equation 4. The right panel gives the integrated profile up to a given angle $\theta_{\rm max}$: $Y_{\rm cyl} = \int_0^{\theta_{\rm max}} 2\pi\theta y(\theta) d\theta$.

0.9 and 5.0. The left panel of Figure 1 gives the Compton parameter y profiles associated to the modeling of the clusters given in table 1, and the right panel gives the integrated Compton parameter $Y_{\rm cyl}$, up to an angular radius $\theta_{\rm max}$, defined by

$$Y_{\rm cyl} = \int_0^{\theta_{\rm max}} 2\pi\theta y(\theta) d\theta \tag{15}$$

Figures 2, 3, 4 and 5 give the Compton parameter y maps and profiles measured versus the one expected (taking into account instrumental lobe and map-making) for some clusters of table 1. These figures are given for 5 hours of observation, with a non correlated noise equal to 2.3 Hz/$\sqrt{\rm Hz}$ in the shift of the resonance frequency TOIs. The electronic correlated noise and the atmospheric noise are simulated as described in Adam et al. (2012), the amplitude of the latter is set to 1 $K_{\rm RJ}$ at 140 GHz and 2.47$K_{\rm RJ}$ at 220 GHz. The plotted errors only takes into account the statistics. In the case of RXJ1347.5-1145, which has a central Compton parameter one order of magnitude above all the other simulated clusters, the profile is well reconstructed (the error plotted are given at a confidence level of 5 σ for graphical convenience). However, in the other cases, we can see the left over correlated noise in the reconstructed maps and the profiles. The scan used here depends on the cluster according to its angular size.

In order to see the best possible measurement (this would be the case for a perfect decorrelation), we simulate observations including only the decorrelated noise. Figures 6 and 7 give the maps and the profiles of two clusters of table 1 in this case. We can see that this time the profile is recovered within the error bars. For 5 hours of observation, in the case of a compact cluster such as those simulated here, we can hope to measure profiles up to a level of $y \gtrsim 10^{-5}$.

6. Conclusions

NIKA should be a powerful instrument for tSZ measurements at high resolution. KIDs arrays have been proved to be competitive detectors for millimeter waves astronomy.

The simulation of the full observation pipeline of galaxy clusters with the NIKA camera at the IRAM 30-meters telescope has shown that the performances of the prototype of NIKA are already good enough to image clusters and measure the pressure profile with a good accuracy within a reasonable time of observation. The Compton parameter y profile injected to simulate observed clusters has been well recovered for the strongest source. Nevertheless, the left over correlated noise is an important bias for the other clusters. In the case of perfect decorrelation, the detection of clusters is expected up to $y \gtrsim 10^{-5}$ with five hours of integration for clusters with a typical angular size of $\sim$ 50 arcsec. The arrays of the final camera should contain about 1000 and 3000 KIDs respectively at 140 and 220 GHz, and it should have a sensitivity as good as the current experiments dedicated to the tSZ effect, such as the South Pole Telescope (Carlstrom et al. (2011)), with a resolution five times better. NIKA appears to be the perfect instrument to perform high resolution follow

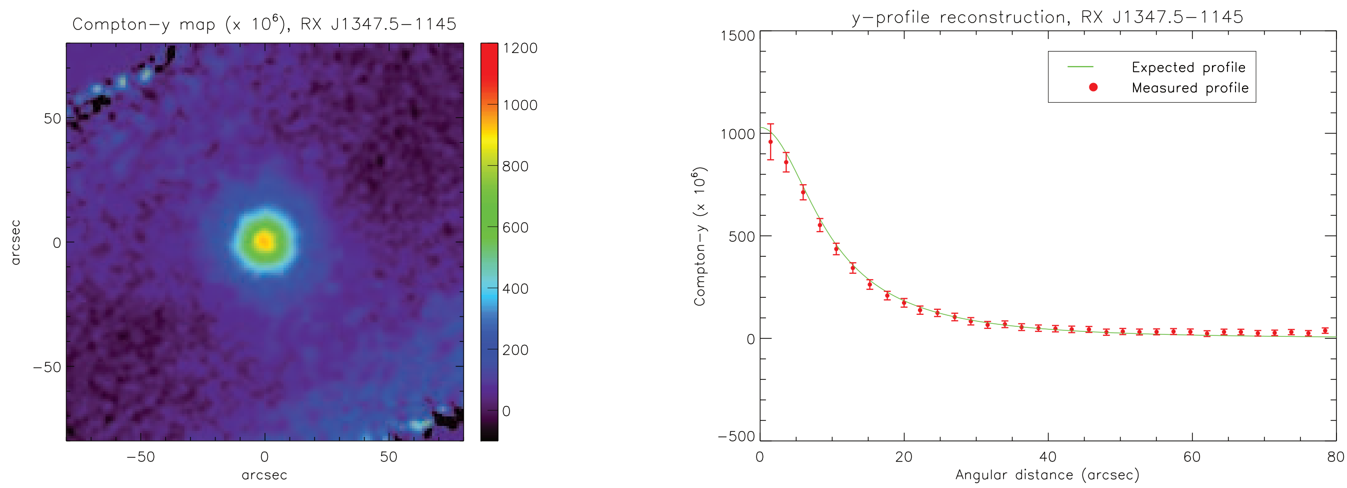

Fig. 2. Recovered Compton parameter y map and profile of the simulation of the cluster RX J1347.5-1145 with all the sources of noise. The given map has been smoothed with a Gaussian of FWHM equal to 5 arcsec. The observation has been simulated according to the observability of the cluster in November 2012, corresponding to 5 hours spread over three days: 2 hours + 2 hours + 1 hour. The path of the scan (serpentine-like scan) used here covers a square with dimensions 210 arcsec × 105 arcsec. The errors are given at the confidence level of 5 σ for graphical convenience.

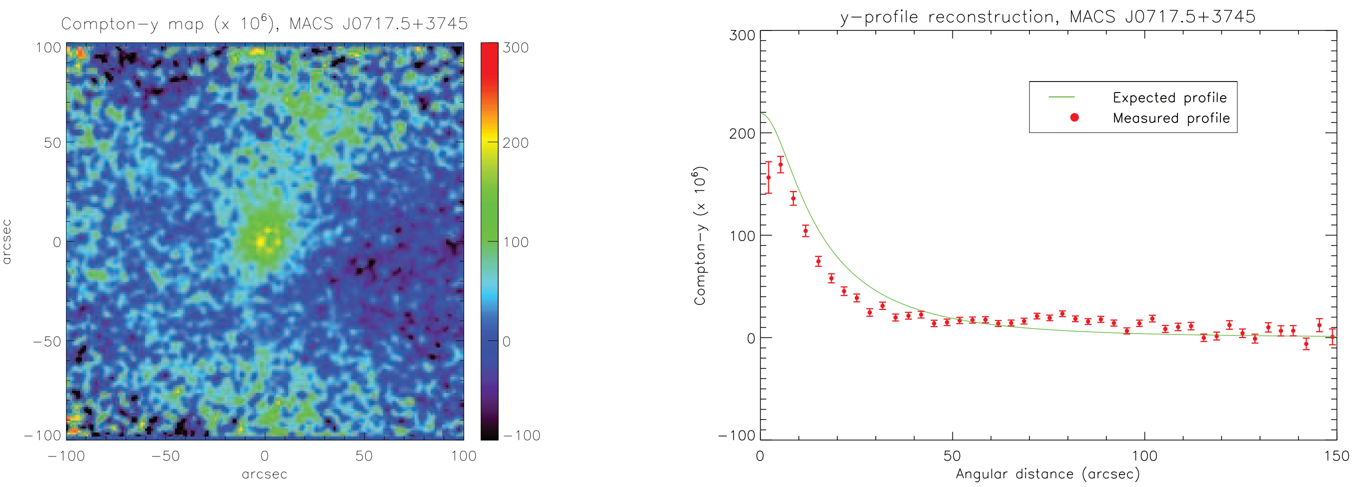

Fig. 3. Recovered Compton parameter y map and profile of the simulation of the cluster MACS J0717.5+3745 with all the sources of noise. The given map has been smoothed with a Gaussian of FWHM equal to 5 arcsec. The observation has been simulated according to the observability of the cluster in November 2012, corresponding to 5 hours without discontinuity. The path of the scan (serpentine-like scan) used here covers a square with dimensions 210 arcsec × 105 arcsec.

ups of clusters detected by Planck (Planck Collaboration et al. (2011), Planck et al. (2012)).

References

Adam, R., Ponthieu, N., Macías-Pérez, J. F., et al. 2012, Research note
AMI Consortium, Shimwell, T. W., Barker, R. W., et al. 2012, MNRAS, 423, 1463
Arnaud, M., Pratt, G. W., Piffaretti, R., et al. 2010, A&A, 517, A92
Benson, B. A., de Haan, T., Dudley, J. P., et al. 2011, ArXiv e-prints
Birkinshaw, M. 1999, Phys. Rep., 310, 97
Borgani, S., Rosati, P., Sartoris, B., et al. 2011, Memorie della Societa Astronomica Italiana Supplementi, 17, 36
Buchert, T. 2008, General Relativity and Gravitation, 40, 467
Calvo, M., Giordano, C., Battiston, R., et al. 2010, Experimental Astronomy, 28, 185
Calvo, M., Roesch, M., Désert, F. X., et al. 2012, A&A
Carlstrom, J. E., Ade, P. A. R., Aird, K. A., et al. 2011, PASP, 123, 568
Carlstrom, J. E., Holder, G. P., & Reese, E. D. 2002, ARA&A, 40, 643
Comis, B., de Petris, M., Conte, A., Lamagna, L., & de Gregori, S. 2011, MNRAS, 418, 1089
Itoh, N., Kawana, Y., Nozawa, S., & Kohyama, Y. 2001, MNRAS, 327, 567
Kosowsky, A. 2003, New A Rev., 47, 939
Larson, D., Dunkley, J., Hinshaw, G., et al. 2011, ApJS, 192, 16
Monfardini, A., Benoit, A., Bideaud, A., et al. 2011, ApJS, 194, 24
Monfardini, A., Swenson, L. J., Bideaud, A., et al. 2010, A&A, 521, A29
Nagai, D., Vikhlinin, A., & Kravtsov, A. V. 2007, ApJ, 655, 98
Planck, AMI Collaborations: N. Aghanim, Arnaud, M., et al. 2012, ArXiv e-prints
Planck Collaboration, Ade, P. A. R., Aghanim, N., et al. 2012, ArXiv e-prints
Planck Collaboration, Ade, P. A. R., Aghanim, N., et al. 2011, A&A, 536, A8
Sunyaev, R. A. & Zel'dovich, Y. B. 1972, Astrophys. Space Phys. Res., 4, 173
Sunyaev, R. A. & Zel'dovich, Y. B. 1980, ARA&A, 18, 537
Tyson, J. A., Wenk, R. A., & Valdes, F. 1990, ApJ, 349, L1

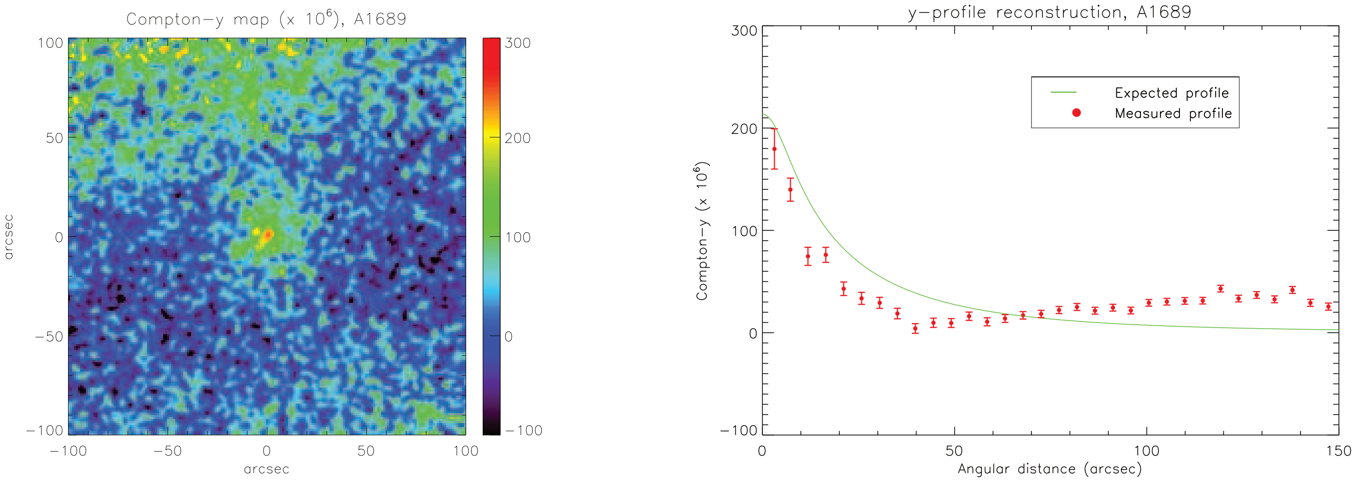

Fig. 4. Recovered y-Compton map and profile of the simulation of the cluster A1689 with all the sources of noise. The given map has been smoothed with a Gaussian of FWHM equal to 5 arcsec. The observation has been simulated according to the observability of the cluster in November 2012, corresponding to 5 hours without discontinuity. The path of the scan (serpentine-like scan) used here covers a square with dimensions 420 arcsec $\times$ 210 arcsec.

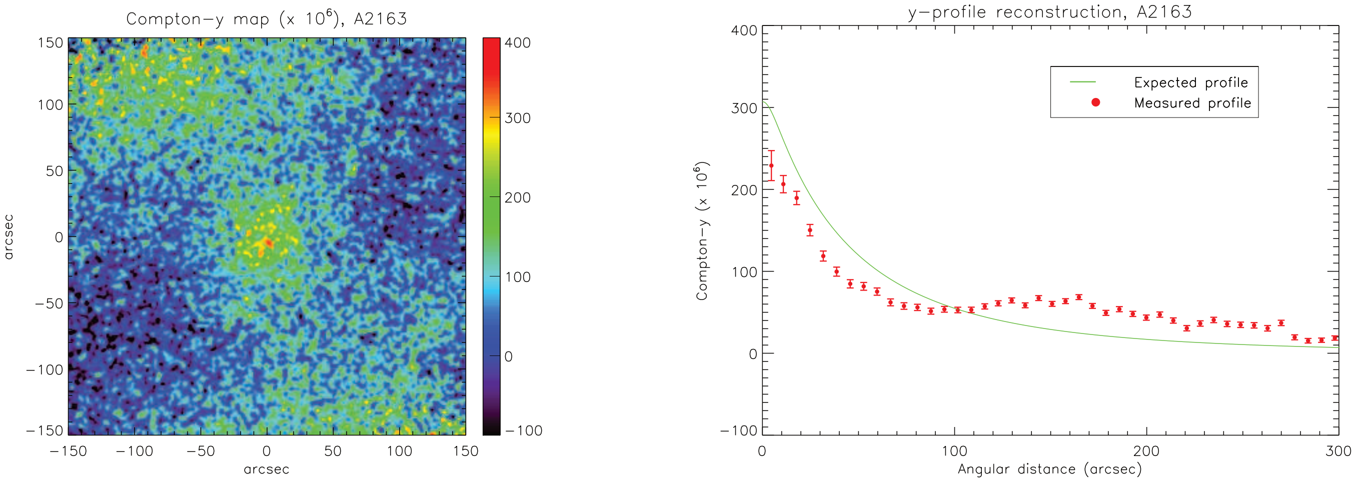

Fig. 5. Recovered Compton parameter y map and profile of the simulation of the cluster A2163 with all the sources of noise. The given map has been smoothed with a Gaussian of FWHM equal to 5 arcsec. The observation has been simulated according to the observability of the cluster in November 2012, corresponding to 5 hours spread over two days: 4 hours + 1 hour. The path of the scan (serpentine-like scan) used here covers a square with dimensions 630 arcsec $\times$ 315 arcsec.

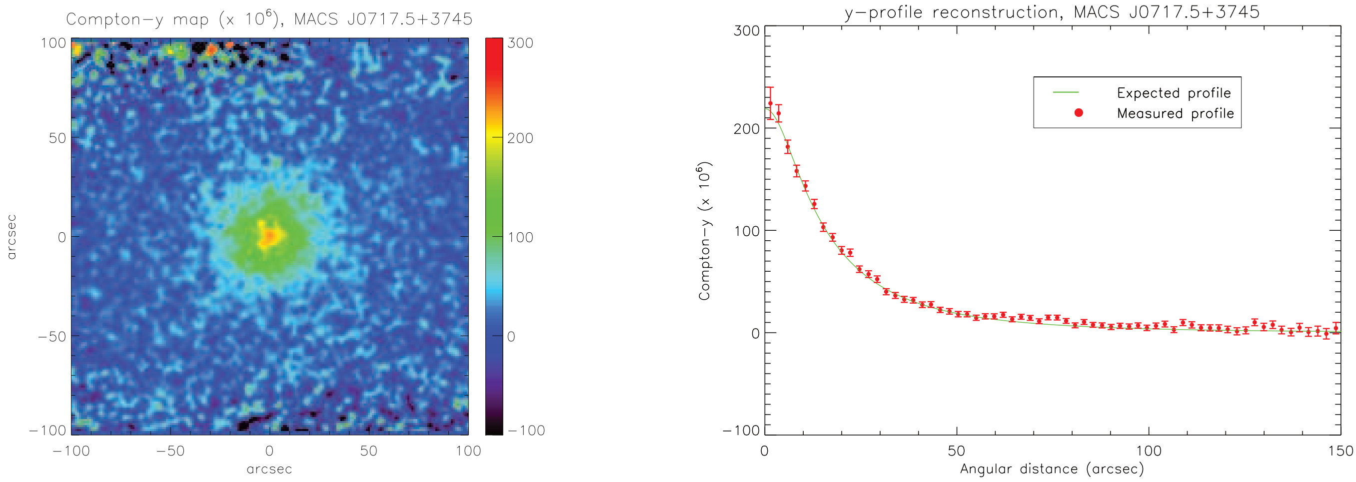

Fig. 6. Recovered Compton parameter y map and profile of the simulation of the cluster MACS J0717.5+3745 with only decorrelated noise. The given map has been smoothed with a Gaussian of FWHM equal to 5 arcsec. The observation has been simulated according to the observability of the cluster in November 2012, corresponding to 5 hours without discontinuity. The path of the scan (serpentine-like scan) used here covers a square with dimensions 210 arcsec × 105 arcsec.

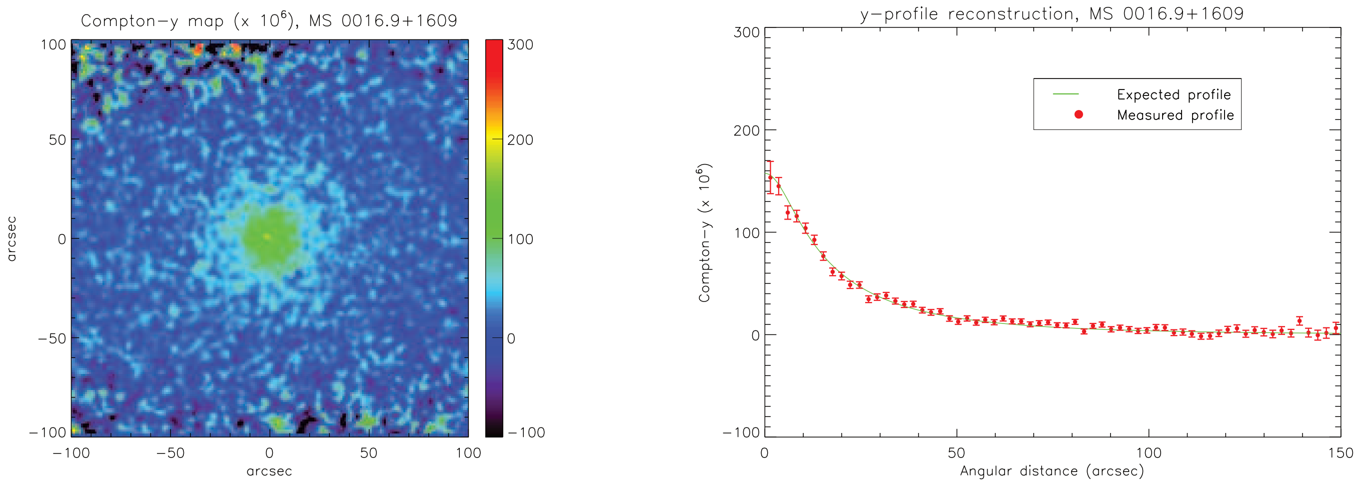

Fig. 7. Recovered Compton parameter y map and profile of the simulation of the cluster MS 0016.9+1609 with only decorrelated noise. The given map has been smoothed with a Gaussian of FWHM equal to 5 arcsec. The observation has been simulated according to the observability of the cluster in November 2012, corresponding to 5 hours without discontinuity. The path of the scan (serpentine-like scan) used here covers a square with dimensions 210 arcsec × 105 arcsec.